

# **Review Article**

# **Journal of Earth Science Biointerfaces**

Volume 1 | Issue 1

# Geophysical and Geochemical Evaluation and Assessment of Subsurface Mineralisation in the Okokoma Area, Cross River State, Southeastern Nigeria

# Chukwuebuka Nnamdi Onwubuariri<sup>1\*</sup>, Istafanus Gwayeri Wasinda<sup>2</sup>, Paul Igienekpeme Aigba<sup>1</sup>, Obinna Christian Dinneya<sup>1</sup>

<sup>1</sup>Michael Okpara University of Agriculture, Department of Physics, Umudike, Abia State, Nigeria

<sup>2</sup>Nigerian Geological Survey Agency, Department of Regional Geology, Jos, Plateau State, Nigeria

\*Corresponding author: Chukwuebuka Nnamdi Onwubuariri, Michael Okpara University of Agriculture, Department of Physics, Umudike, Abia State, Nigeria

**Citation:** Chukwuebuka Nnamdi Onwubuariri (2025) Geophysical and Geochemical Evaluation and Assessment of Subsurface Mineralisation in the Okokoma Area, Cross River State, Southeastern Nigeria. J Earth Sci Bioin 1(1): 1-11.

Received Date: November 01, 2025 Accepted Date: November 11, 2025 Published Date: November 20, 2025

#### **Abstract**

This research employs Vertical Electrical Sounding (VES) and X-ray Fluorescence (XRF) spectroscopy to thoroughly characterise the shallow to moderate subsurface of the Okokoma area in Obubra L.G.A., Cross River State, Nigeria. The Abakaliki Anticlinorium, located in the Pb-Zn mineralised zone of the Benue Trough, exhibits a complex tectonic history that facilitates the formation of hydrothermal ore deposits. Traditional mapping frequently fails to provide comprehensive subsurface information, requiring the use of advanced investigative methods. The non-invasive VES method, which used a Schlumberger array at seven sites, effectively identified four distinct geoelectric layers. Results indicated notable variations in apparent resistivity with depth, corresponding to lithological changes from high-resistance arid topsoil and lateritic layers to conductive clayey and weathered shales at intermediate depths and more compact, potentially mineralised formations at greater depths. Certain VES points displayed significantly high resistivity anomalies, suggesting the presence of lead-zinc mineralisation. In addition, precise geochemical analysis of rock samples through XRF spectroscopy, employing the Fundamental Parameters (FP) method, yielded detailed elemental and oxide compositions. The depositional environment was dominated by oxides like SiO<sub>2</sub>, Fe<sub>2</sub>O<sub>3</sub>, and Al<sub>2</sub>O<sub>3</sub>. It's also clay-rich. Although the geochemical presence of PbO, ZnO, and CdO, as well as traces of Au and Cu, suggests mineralisation, they do not invariably indicate hydrothermal alteration. Comparing mineral alteration features and whole-rock geochemistry in obviously altered and unmodified samples improved the reliability of hydrothermal alteration identification. Given the sedimentary setting, mineralisation was recognised as sediment-hosted with a syngenetic or diagenetic origin, which was not ruled out without more mineralogical and geochemical data. The integration of geophysical anomalies and geochemical signatures enhances our understanding

Keywords: Vertical electrical sounding, Mineralization, X-ray Fluorescence, Abakaliki Anticlinorium, Resistivity, Spectroscopy

#### **Highlights**

- A geophysical-geochemical approach was used to combine vertical electrical sounds (VES) with X-ray fluorescence (XRF) spectroscopy to determine subsurface conditions and mineralisation potential in the studied area. This integrated approach enabled cross-validation and stronger interpretation.
- Detailed Subsurface Resistivity Characterisation: VES surveys found significant variations in apparent resistivity values across depths and locations, correlating these anomalies with dry sandy overburdens, lateritic layers, weathered clay/ shales, and more compact, potentially mineralised rocks.
- Geophysical Signatures of Pb-Zn Mineralisation: VES 1, 2, 3, 5, 6, and 7 showed continuous patterns of rising resistivity at deeper layers, strongly confirming the presence of mineralised zones, specifically Pb-Zn mineralisation. These anomalies indicate fractured/faulted zone silicification, carbonate alteration, or mineralisation.
- Geochemical Confirmation of Polymetallic Mineralisation:

- Pit sample XRF analysis confirmed geophysical findings. PbO, ZnO, CdO, and sometimes CuO and Au were found in high concentrations, suggesting polymetallic (Pb-Zn) mineralisation.
- Geochemical data revealed hydrothermal alteration, including elevated Fe<sub>2</sub>O<sub>3</sub>, Al<sub>2</sub>O<sub>3</sub>, K<sub>2</sub>O, and the presence of chlorine (Cl) and sulphur trioxide (SO<sub>3</sub>), indicating mineralising fluids' role in rock formation and ore genesis.
- Mineralisation and Geological Structures: Geophysical and geochemical data imply that the Abakaliki Anticlinorium's mineralisation is linked to structural controls, including fractures, faults, and significant hydrothermal activity.

#### Introduction

This study conducts a comprehensive analysis of the Okokoma area in the Obubra Local Government Area, Cross River State, Nigeria. The study area, situated in the Abakaliki Anticlinorium (figure 1), a significant geological formation in the Benue Trough

J Earth Sci Bioin, 2025 Page 1 of 11

in southeastern Nigeria, is recognised for its considerable lead-zinc (Pb-Zn) mineralization. The complex tectonic processes in this region, characterised by notable folding, faulting, and magmatic intrusions, have created favourable conditions for the formation of hydrothermal ore deposits. Understanding the subsurface characteristics and distribution of valuable mineral resources is key for both theoretical insights into ore genesis and practical applications in mineral exploration [1-4].

Traditional geological mapping often provides inadequate information about deeper subsurface structures and the precise locations of ore bodies. Therefore, the incorporation of sophisticated subsurface investigation methods is crucial. This study employs a multidisciplinary approach, combining Vertical Electrical Sounding (VES), a non-invasive geophysical technique, with X-ray Fluorescence (XRF) spectroscopy, a precise geochemical analytical method. The VES method effectively detects variations in subsurface electrical resistivity, which may correlate with different lithologies, fluid contents, and the potential presence of conductive or resistive mineralised zones. XRF analysis of rock samples provides comprehensive elemental and oxide compositions, offering direct geochemical signatures of mineralisation and associated alteration processes [5-10]. This is made possible because. Hydrothermal fluids transport mineralised elements across deep fractures, faults, and porous zones, causing chemical changes in the surrounding rocks. These flows move these elements upward, creating surface enrichment that reflects beneath ore deposits. Surface patterns and spatial correlations of pathfinder elements (e.g., Pb, Zn, Cu, Au) frequently map the extent and position of deeper mineralised zones. Furthermore, fault zones and fractures serve as conduits for mineralising fluids. Surface geochemical anomalies are widespread along these structures, which can also be seen in geophysical surveys, establishing strong spatial linkages between surface chemistry and subsurface structures.

Previous studies have given us clues to regional tectonics and mineralisation; however, challenges remain in thoroughly characterising subsurface structures and precisely delineating mineralisation zones. This study aims to fill the existing gap by employing integrated geophysical and geochemical methods to characterise subsurface geoelectric layers and validate indicators of mineralisation, thereby enhancing targeting for mineral exploration. Table 1 indicates the coordinates of the study areas.

**Table 1: Table of Geophysical Survey Points** 

|      |                      | •        |           |
|------|----------------------|----------|-----------|
| S/No | VES/PIT<br>LOCATIONS | LATITUDE | LONGITUDE |
| 1    | 1                    | 6.098370 | 8.398067  |
| 2    | 2                    | 6.096907 | 8.412808  |
| 3    | 3                    | 6.094465 | 8.420813  |
| 4    | 4                    | 6.086228 | 8.424740  |
| 5    | 5                    | 6.081318 | 8.425508  |
| 6    | 6                    | 6.092316 | 8.414211  |
| 7    | 7                    | 6.088588 | 8.417897  |

#### Geological Background of the Area

Okokoma, located in the Obubra Local Government Area of Cross River State, lies within the Benue Trough, which is renowned for its natural resources, notably lead, zinc, and various base metals. The region's geology is predominantly made up of sedimentary rocks, with occasional igneous intrusion and accompanying contact metamorphism of the surrounding sedimentary country rocks. The region is supported by shale, sandstone, and limestone rocks, which are frequently linked to mineralisation zones. These

rocks create an appropriate environment for the production and concentration of Pb–Zn mineralization [11-14]. Figure 2 depicts the geologic map of the study area and environs. The research area primarily comprises sediment-hosted Lead-Zinc (Pb-Zn) deposits, displaying mineralisation types that range from syngenetic to hydrothermal origins. Structural controls, such as faults and fractures, enable the movement of mineralising fluids, thus enhancing ore concentration within the Abakaliki Formation and related units. A thorough characterisation of these structural properties is essential for understanding mineral deposition.

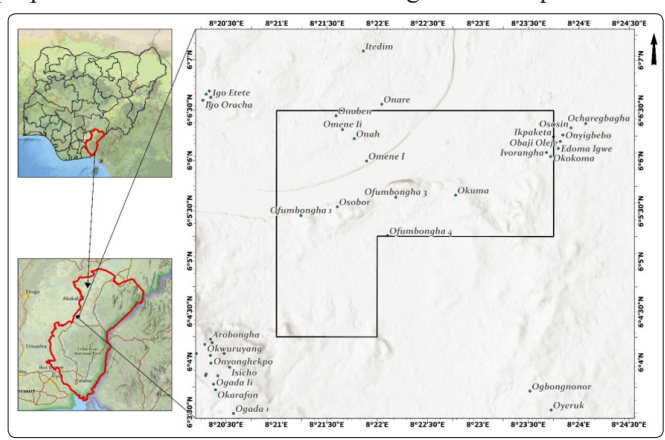


**Figure 1:** Location map of the study area (Obubra) Part of Sheet 303 (Abakaliki)

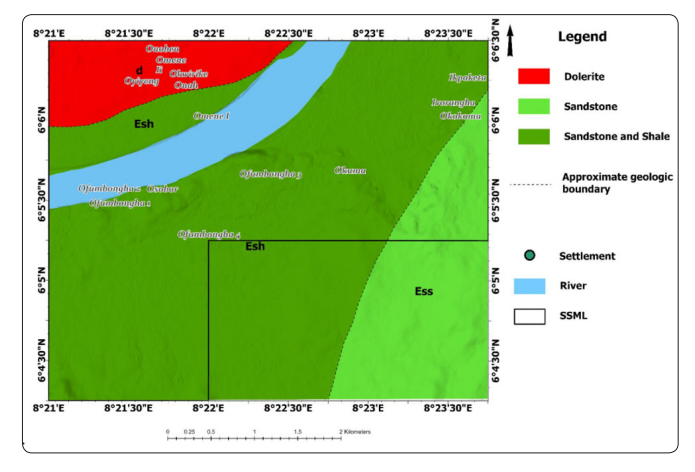


**Figure 2:** Geologic map of Obubra and environs, Part of Sheet 303 (Abakaliki). The geologic data is extracted from Geologic map of Nigeria (1:2,000,000) (NGSA, 2010).

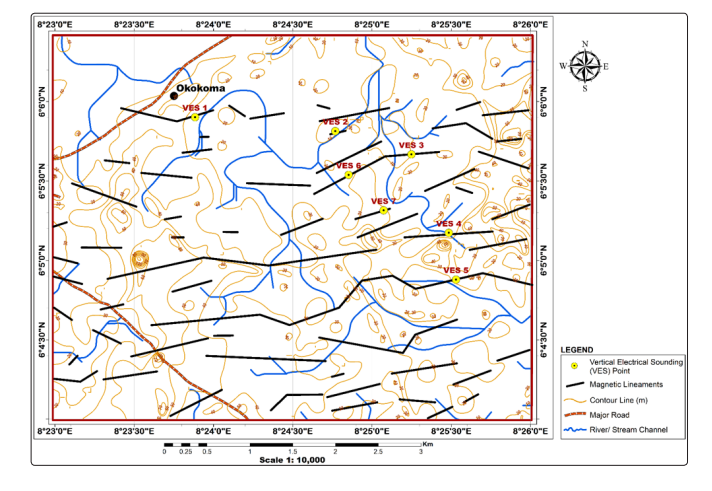


**Figure 3:** Map indication VES positions on magnetic lineament map of the study area

J Earth Sci Bioin, 2025 Page 2 of 11

#### Methodology

This study employed geophysical and geochemical methods. In the geophysical approach, Vertical Electrical Soundings (VES) were utilised, while for the geochemical aspect, X-ray Fluorescence (XRF) spectroscopy was applied in alignment with the Fundamental Parameters (FP) method for quantitative analysis.

# Geophysical method – Vertical Electrical Soundings

This investigation utilised Vertical Electric Sounding (VES), a geophysical exploration technology. VES operates by correlating the subsurface electrical characteristics of the studied region [3, 15]. The subsurface electrical characteristics are detected by the resistivity variations among the various rock types and lithologies in the region. The VES provides extensive information on the vertical arrangement of several conductive zones. The measurements utilise four electrode arrays, comprising two current electrodes and two potential electrodes (Schlumberger Array), with the Campus Ohmega Resistivity Meter [5].

The VES approach utilised the Schlumberger electrode configuration, with the electrode spacing (AB/2) varying from 1.5 m to 125 m. A total of seven VES locations were distributed throughout the study region. Each VES curve was presented alongside field and synthetic curves to ascertain resistivity at different depths. The field measurement data were juxtaposed with synthetic models to corroborate the geophysical findings. Figure 3 indicates the VES positions within the study area and figure 4 illustrates the configuration of a Schlumberger array.

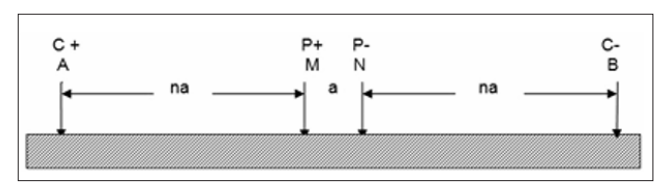


Figure 4: Schlumberger array

## **Geochemical Analysis**

Solid bulk materials, regarded as homogeneous solids, were collected from pits dug at various VES positions (a total of seven), where thickness corrections were considered unnecessary. Surface geochemical data collected are spatially associated with geophysical surveys such as Vertical Electrical Sounding (VES), which offers indirect measurements of subsurface resistivity. High elements concentration patterns in surface samples that correspond spatially with geophysical anomalies point to underlying mineralisation. It is also worth noting that surface sample locations were determined by known or inferred geological structures (faults, folds) and lithologies. These structural restrictions frequently extend into the subsoil. As a result, surface anomalies over structural features indicate probable mineralised zones that extend to depth. This geochemical sampling method involved collecting bulk solids at a depth of 3 meters from each VES site to ensure spatial correlation with geophysical anomalies.

Samples were collected by employing standardised methods to avoid contamination. Quality control was achieved via numerous analyses and calibrations that utilised verified reference materials. Geophysical and geochemical techniques are outlined in multiple sections for clarity.

The fundamental and oxide configurations of the samples were analysed using X-ray Fluorescence (XRF) spectroscopy, employing the Fundamental Parameters (FP) method for quantitative assessment. XRF is a non-destructive method commonly employed to determine the primary concentrations of solid materials by measuring the characteristic secondary (fluorescent) X-rays released from atoms when stimulated by a primary X-ray source [16-17].

This analysis utilised the following instrument parameters: rhodium (Rh) as the X-ray source target, a power source of 30 kV and 30  $\mu A$  for the excitation voltage and current, a silicon drift detector (SDD) as the detector type, and ambient air as the atmosphere. These parameters were employed to enhance detection sensitivity across a broad spectrum of elements, particularly those prevalent in geological and environmental matrices.

Detected elements were documented for raw intensity data represented in counts per second (c/s). The FP technique facilitated the conversion of these intensities into quantitative concentrations. This technique corrects for matrix effects, such as absorption and enhancement, thereby influencing fluorescence yields in relation to sample configuration. The FP method provides a more consistent and precise quantification than the experiential calibration technique, particularly in varying or complex matrices [18].

#### **Results and Discussion**

To determine the reliability of the resistivity data, a statistical analysis was performed. This analysis included calculating the mean, standard deviation, and uncertainty estimates. Overlay maps were used in the supplemental material to see how geochemical element concentrations are related to geophysical resistivity anomalies. Detailed captions have been added to the figures to enhance their readability. The geochemically discovered environmental impacts of heavy metals (Pb, Cd, and Cu) were discussed in terms of possible contamination risks and recommendations for monitoring.

#### **Geophysical Analysis**

The vertical electrical soundings (VES) indicated that the apparent resistivity values at various VES points, beginning with the topsoil, exhibit considerable variation. The variation indicates the existence of various types of formations and potentially the presence of additional components and factors that may influence the apparent resistivity values of rock layers, either enhancing or diminishing them. Table 2 presents a comprehensive summary of the resistivity values obtained during the research process.

J Earth Sci Bioin, 2025 Page 3 of 11

Table 2: Summary of VES 1 to 7 apparent resistivity measurement

| AB/2 | Apparent Resistivity |        |        |        |        |        |        | Average                 |
|------|----------------------|--------|--------|--------|--------|--------|--------|-------------------------|
|      | VES 1                | VES 2  | VES 3  | VES 4  | VES 5  | VES 6  | VES 7  | Apparent<br>Resistivity |
| 1.5  | 138.56               | 21.861 | 11.533 | 411.45 | 32.737 | 136.72 | 130.72 | 126.2258571             |
| 2    | 117.89               | 15.893 | 8.5668 | 329.84 | 28.802 | 85.807 | 75.807 | 94.65797143             |
| 2.6  | 71.632               | 13.48  | 8.4053 | 271.99 | 26.393 | 65.756 | 65.756 | 74.77318571             |
| 3.4  | 53.873               | 13.915 | 8.6594 | 256.03 | 21.162 | 50.142 | 70.142 | 67.70334286             |
| 4.5  | 30.064               | 18.374 | 9.3718 | 196.89 | 18.842 | 29.699 | 29.699 | 47.56282857             |
| 6    | 25.658               | 22.227 | 10.869 | 125.7  | 16.627 | 27.798 | 25.798 | 36.38242857             |
| 8    | 19.907               | 24.557 | 12.398 | 93.062 | 15.698 | 17.948 | 19.948 | 29.074                  |
| 10.5 | 17.786               | 25.247 | 14.443 | 53.86  | 15.33  | 16.64  | 15.65  | 22.70657143             |
| 14   | 14.223               | 24.336 | 17.338 | 26.853 | 14.972 | 14.598 | 15.598 | 18.274                  |
| 18   | 14.354               | 22.991 | 20.217 | 20.589 | 14.434 | 14.535 | 15.535 | 17.52214286             |
| 24   | 14.899               | 16.234 | 19.988 | 18.337 | 14.36  | 12.805 | 14.805 | 15.91828571             |
| 32   | 17.822               | 17.101 | 17.065 | 17.013 | 16.144 | 11.687 | 13.687 | 15.78842857             |
| 42   | 20.571               | 16.294 | 13.679 | 17.107 | 17.747 | 10.79  | 12.79  | 15.56828571             |
| 55   | 20.92                | 14.46  | 13.5   | 18.64  | 21.24  | 10.4   | 12.4   | 15.93714286             |
| 72.5 | 20.11                | 12.95  | 13.63  | 20.56  | 26.13  | 9.54   | 12.54  | 16.49428571             |
| 95   | 13.87                | 12.74  | 11.44  | 20.61  | 30.52  | 12.68  | 10.66  | 16.07428571             |
| 125  | 12.81                | 11.81  | 9.35   | 21.46  | 32.89  | 17.66  | 15.67  | 17.37857143             |

The average apparent resistivity values shown in Table 2 provide a general overview of the resistivity ranges obtained at various depths and VES locations. These averages help to provide an initial grasp of the research area's overall resistivity characteristics. However, they do not reflect the complete geographic variability and local variation that exists at individual VES locations.

#### **Analysis of Resistivity Trends**

The observed pattern of apparent resistivity as electrode spacing (AB/2) increases demonstrates a general decrease in resistivity from shallow to intermediate depths, subsequently stabilising at greater depths. At near surface depths (1.5 m to 6.0 m being the range of AB/2), the values of resistivity are moderately high, having readings between approximately 127 and 36 ohm-m. This form agrees with the presence of dry, consolidated topsoil, lateritic strata, or sandy materials. VES 4 reveals a substantial resistivity of 411.45 ohm-m at a depth of 1.5 m, signifying the probable presence of dry, unconsolidated sand or gravel close to the top. As we go deeper the subsurface, (AB/2 from 6.0 m to approximately 24.0 m), resistivity values show a clear drop from 28.79 to 15.63 ohm-m. The low-resistivity zone mostly contains clayey or weathered minerals, conceivably weathered shale or siltstone—known for their conductivity ascribed to their mineral structure and damp nature. Resistivity values settle beyond a depth of 24.0 m, ranging somewhat between 15.5 and 17.7 ohm-m up to the maximum depth of 125.0 m for AB/2. The approximately equal resistivity shows a comparable underlying configuration, probably containing saturated compact shale or mudrock with partial fracture. The resistivity pattern shows a shift from dry surface constituents to more conductive, worn, and compact geological formations at increased depths.

#### Geoelectric Strata and Lithological Correlation

The resistivity distribution with depth, as presented in Table 3, reveals that the subsurface of the research area comprises four main geoelectric layers as shown in figure 5. The upper layer, extending from the surface to approximately 3 meters in depth, demonstrates increased resistivity values between 100 and 127 ohm-m. This layer is probably made-up of lateritic topsoil, arid consolidated sand, or gravel. The second layer, at a depth of about 3 to 8 meters, exhibits moderate resistivity values of 50–75 ohm-m and is possibly made-up of sandy clay, silty clay, or moderately weathered shale. The third layer, situated at depths of 8 to 25 meters, displays meaningfully lower resistivity values (15–30 ohm-m), representing a zone characterised by weathered shale or cracked clay-rich formations. This layer likely acts as the core aquifer unit, though its clayey configuration may limit groundwater production. The fourth layer, covering 25 meters to over 125 meters, parades a comparatively constant low resistivity of 15–18 ohm-m, signifying the occurrence of wet compact shale, mudrock, or weakly cracked bedrock. The results agree with the already existing lithological forms in the Abakaliki Formation and are consistent with previous geophysical and hydrogeological studies in the Lower Benue Trough.

Apparent resistivity was computed from field measurements of voltage and current using Ohm's Law, then modified by a geometric factor appropriate to the electrode array arrangement and spacing using the formula:

$$\rho_a = K \times \frac{V}{I} \tag{1}$$

where  $\rho_a$  is the apparent resistivity, V is the measured potential difference between potential electrodes, I, is the current injected into the ground by current electrodes, and K, is a geometric factor that accounts for electrode spacing and positioning, typically derived from distances between electrodes as:

$$K = 2\pi \left(\frac{1}{r_{AM}} - \frac{1}{r_{BM}} - \frac{1}{r_{AN}} + \frac{1}{r_{BN}}\right)^{-1} \tag{2}$$

J Earth Sci Bioin, 2025 Page 4 of 11

Here, r<sub>xy</sub> are distances between electrodes (A, B for current, M, N for potential).

| Layer | Depth Range<br>(approx.) | Apparent Resistivity (Ωm) | Interpretation   |
|-------|--------------------------|---------------------------|--|
| 1     | 0–3 m                    | 100–127                   | Lateritic topsoil or dry compact sand  |
| 2     | 3–8 m                    | 50–75                     | Sandy clay or silty clay (partially weathered shale)                           |
| 3     | 8–25 m                   | 15–30                     | Weathered/faulted shale, water-bearing potential                               |
| 4     | 25–125+ m                | 15–18                     | Fractured shale or saturated compacted mudrock (low-yield aquifer or aquitard) |

Table 4: Average Apparent Resistivity Values for Interpreted Geoelectric Layers Across VES Points

| VES | Latitude | Longitude | Average Apparent Resistivity for Layer Ranges |                |                 |                    |
|-----|----------|-----------|---|----------------|-----------------|--------------------|
|     |          |           | Layer 1 (0–3m)                                | Layer 2 (3–8m) | Layer 3 (8–25m) | Layer 4 (25–125+m) |
| 1   | 6.09837  | 8.398067  | 109.3606667                                   | 32.3755        | 15.3155         | 17.68383333        |
| 2   | 6.096907 | 8.412808  | 17.078  | 19.76825       | 22.202          | 14.22583333        |
| 3   | 6.094465 | 8.420813  | 9.5017  | 10.32455       | 17.9965         | 13.11066667        |
| 4   | 6.086228 | 8.42474   | 337.76  | 167.9205       | 29.90975        | 19.23166667        |
| 5   | 6.081318 | 8.425508  | 29.31066667                                   | 18.08225       | 14.774          | 24.11183333        |
| 6   | 6.092316 | 8.414211  | 180.09433333                                  | 30.39675       | 14.6445         | 6.12616667         |
| 7   | 6.088588 | 8.417897  | 42.09433333                                   | 12.39675       | 40.6445         | 35.12616667        |

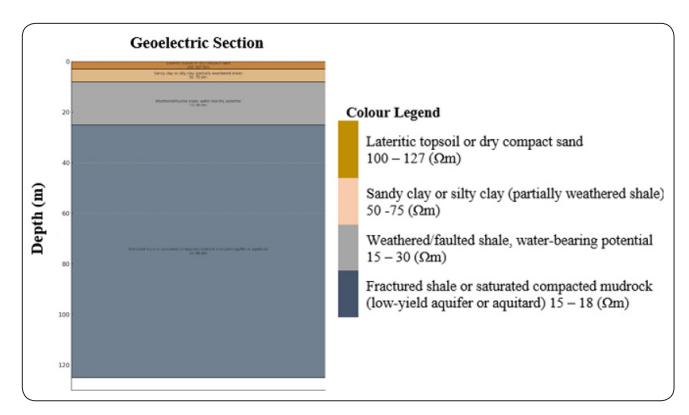
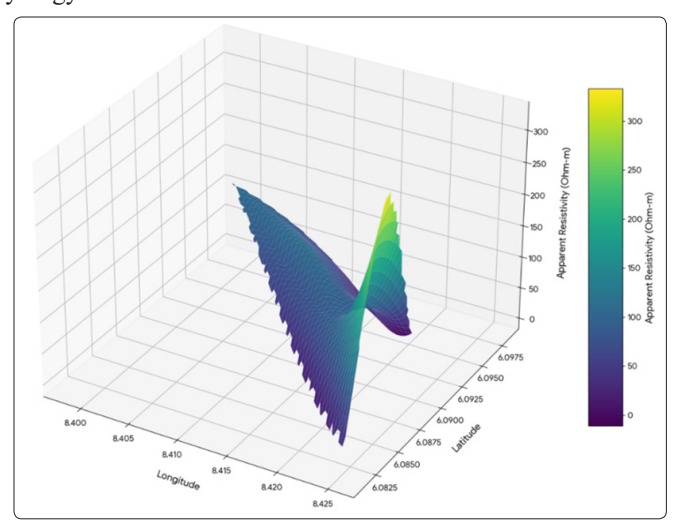
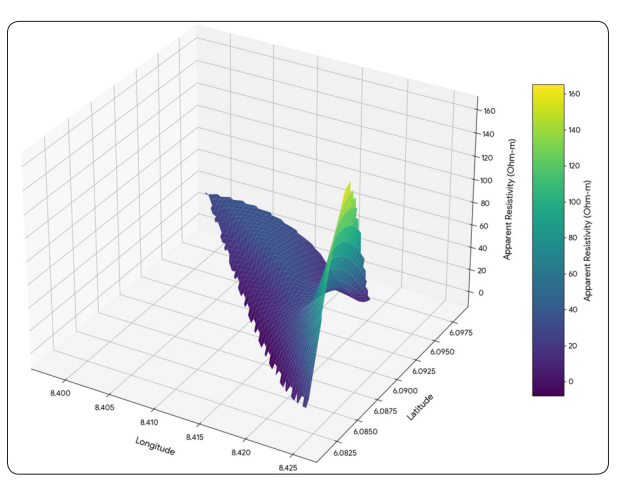


Figure 5: Diagram of Geoelectric section of the study area

Figures 6, 7, 8 and 9 represents the 3D expression of layer 1 of all the VES points, Layer 2 of all the VES points, Layer 3 of all the VES points and Layer 4 of all the VES points respectively in synergy with Table 4.



**Figure 6:** 3D map for Layer 1 (0–3 m) showing the apparent resistivity distribution across the VES locations



**Figure 7:** 3D map for Layer 1 (3-8 m) showing the apparent resistivity distribution across the VES locations.

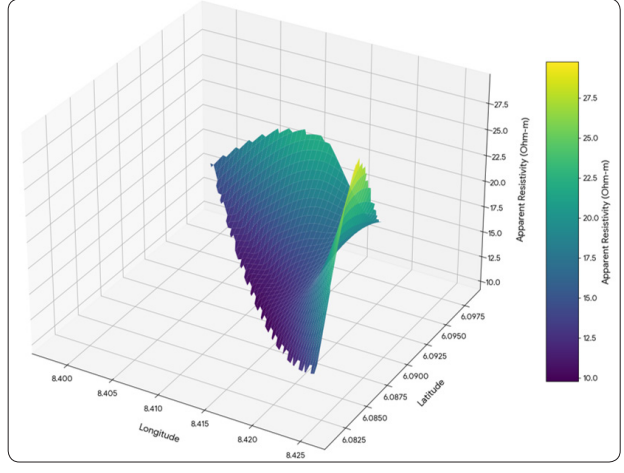


**Figure 8:** 3D map for Layer 1 (8-25 m) showing the apparent resistivity distribution across the VES locations.

J Earth Sci Bioin, 2025 Page 5 of 11

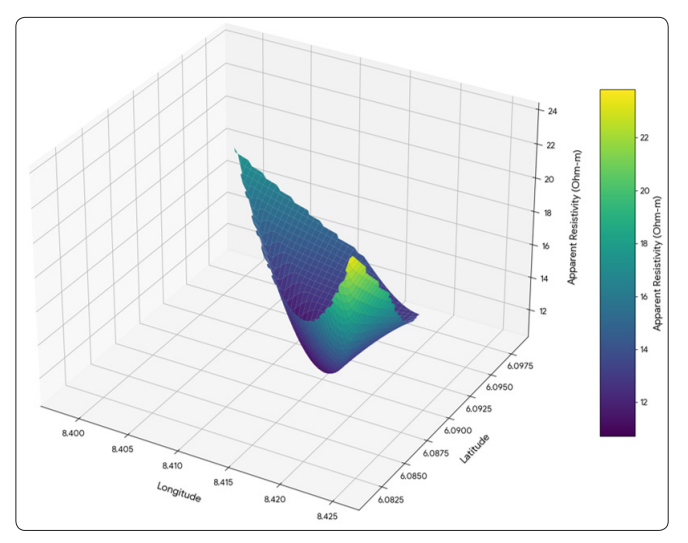


**Figure 9:** 3D map for Layer 1 (25-125+ m) showing the apparent resistivity distribution across the VES locations.

#### **VES 1 Signature Analysis**

A resistivity value of approximately 203.19  $\Omega m$  was recorded at the top layer of VES 1, indicating the presence of dry sandy overburden and a lateritic layer. A resistivity value of 7.3  $\Omega m$  was recorded at the middle layer, suggesting the presence of a potentially weathered clay zone with a reduced rate of water evaporation. The resistivity value of the deeper layer increased slightly to 71.18  $\Omega m$ , indicating the potential presence of more compacted, possibly mineralised rocks. The transition from higher to lower resistivity at greater depths indicates the presence of mineralised rock, which is associated with Pb-Zn mineralisation. Figure 10 presents the relationship between AB/2 and apparent resistivity at the VES 1 location.

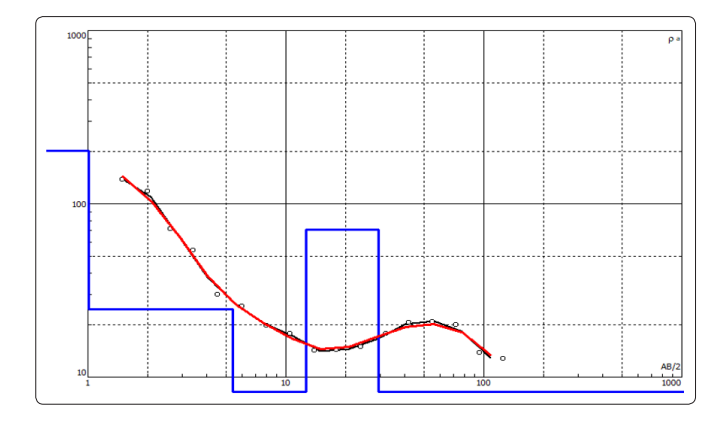


Figure 10: Plot of AB/2 versus Apparent Resistivity for VES 1

# **VES 2 Signature Analysis**

A resistivity value of 35.87  $\Omega$ m was recorded at the upper layer of the VES 2 location. The middle layer exhibited a significant decrease in resistivity value (3.46  $\Omega$ m), indicating the presence of wet clay or a shaly zone. At the deeper layer, a significant increase in the resistivity value (135  $\Omega$ m) was observed, with minor fluctuations as depth increased. The not to high resistivity values indicates the presence of a mineralised zone, likely containing lead or zinc ores. The presence of a conductive material and possibly trapped fluid within the middle layer resulted in a very low resistivity value, while a higher resistivity value observed at deeper

layers which could be as a result of compaction and lack of fluid within the layer to dissolved some minerals present. The resistivity value observed in the deeper layer, which is moderately low, indicated the existence of cracked or mineral-rich rock deposits. Figure 11 presents the relationship between AB/2 and apparent resistivity at the VES 2 location.

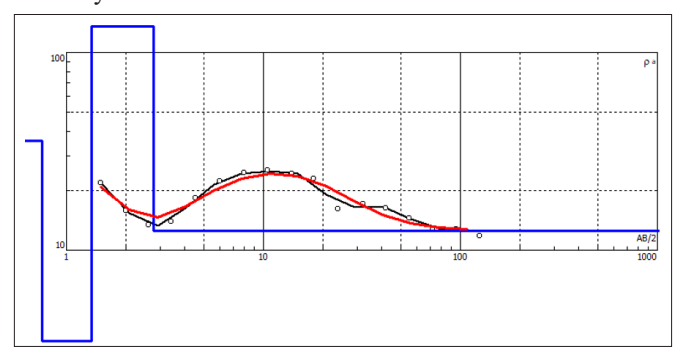


Figure 11: Plot of AB/2 versus Apparent Resistivity for VES 2

#### **VES 3 Signature Analysis**

A low resistivity value of approximately 15.96  $\Omega$ m was recorded at the topsoil, indicating the presence of clay and moist saturated sediments. The middle layers exhibited a resistivity value reduction to 5.17  $\Omega$ m, consistent with clayey or weathered formations. Deeper dry layers show a modest rise in resistivity to 57.23  $\Omega$ m, indicating a probable Pb-Zn mineralisation zone. This is likely due to fractures or strain features in the substrate. Figure 12 presents the relationship between AB/2 and apparent resistivity at the VES 3 location.

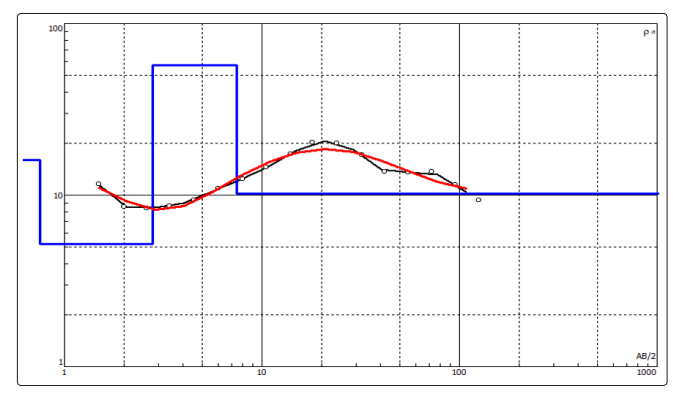


Figure 12: Plot of AB/2 versus Apparent Resistivity for VES 3

#### **VES 4 Signature Analysis**

The resistivity of topsoil at the VES 4 position is the highest among the topsoil resistivities recorded at other VES points in this study. A resistivity value of approximately 546  $\Omega m$  was observed in the topsoil, indicating a compressed, dry, and solid overburden, potentially laterite. The resistivity values of the middle layers decreased to an average of 228.5  $\Omega m$ . A significant drop in resistivity (15.77  $\Omega m$ ) was observed at deeper layers, indicating a sharp transition to lower values, which suggests the presence of conducting minerals (Pb-Zn) in substantial volumes and possibly fluids, which most have dissolved some components of the mineral to reduce the resistivity of the layer. The resistivity anomaly detected at greater depths indicates a significant presence of ore minerals, likely associated with Pb–Zn mineralisation. Figure 13 presents the relationship between AB/2 and apparent resistivity at the VES 4 location.

J Earth Sci Bioin, 2025 Page 6 of 11

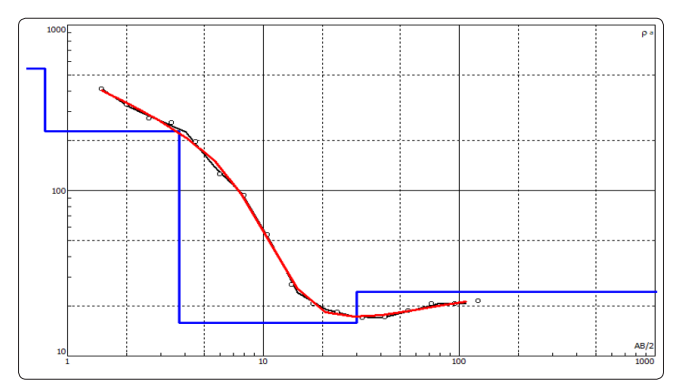


Figure 13: Plot of AB/2 versus Apparent Resistivity for VES 4

#### **VES 5 Signature Analysis**

At the VES 5 position, the resistivity of the topsoil was measured at approximately 36.15  $\Omega$ m, indicating a slightly sandy texture or a not overly dry overburden. The average resistivity of the middle layers is 14.11  $\Omega$ m, indicating a decrease that suggests the presence of clay or weathered layers. Increased resistivity values were observed in deeper layers, reaching a peak of 81.11  $\Omega$ m. This also uncovers a promising subsurface region that may serve as an excellent mineral prospect. The increase in resistivity with deeper penetration indicated the presence of mineralised zones, potentially associated with Pb–Zn ores found in fractured or veinhosted structures. Figure 14 illustrates the relationship between AB/2 and apparent resistivity at the VES 5 location.

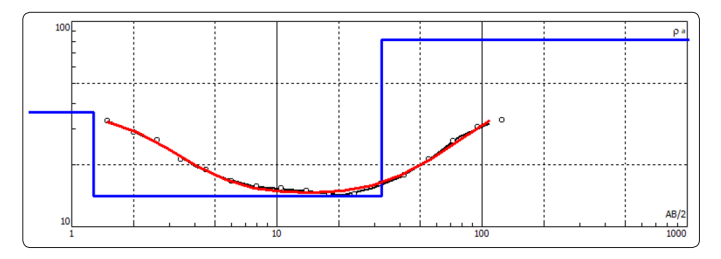


Figure 14: Plot of AB/2 versus Apparent Resistivity for VES 5

#### **VES 6 and VES 7 Signature Analysis**

The VES positions displayed significant similarities in their respective resistivity values. Resistivity measurements of 136.72 and 130.72  $\Omega m$  were obtained at the upper layers respectively, suggesting the presence of dry, compacted overburden. The resistivity values of their middle layers are 14.598 and 15.598  $\Omega m$  respectively, which is in consonant with table 2, indicating the presence of weathered or clayey materials. Subsequent layers exhibited a resistivity value of not less than 10  $\Omega m$ , signifying distinct mineralised zones in the subsurface, specifically related to Pb–Zn mineralisation. The significant resistivity variation at greater depths indicates a mineralised zone, which is potentially indicative of lead and zinc mineralisation. Figures 15 and 16 illustrate the relationship between AB/2 and apparent resistivity at VES positions 6 and 7.

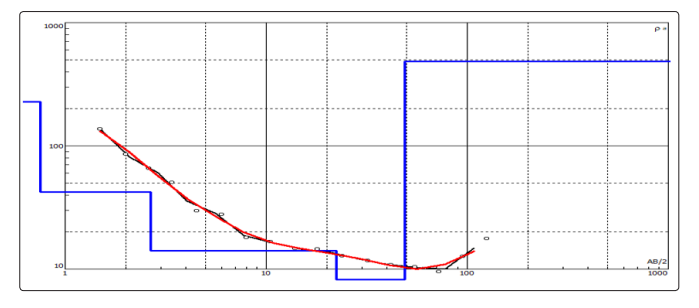


Figure 15: Plot of AB/2 versus Apparent Resistivity for VES 6

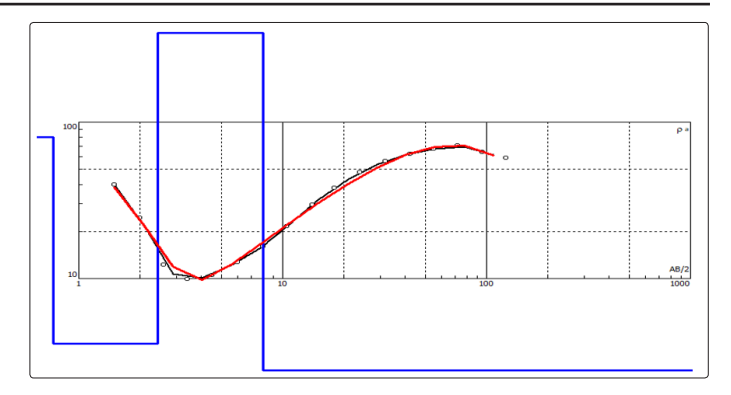


Figure 16: Plot of AB/2 versus Apparent Resistivity for VES 7

#### **Curve Implication**

An integrated analysis integrating vertical electrical sounding (VES) data with established geological understanding of the Abakaliki Anticlinorium provides support for the interpretation of resistivity anomalies as markers of fault connections or mineralised veins. The resistivity distribution patterns presented in Figures 6-16 demonstrate localised high to low resistivity zones that spatially correlate with known structural elements, such as faults and fractures, determined through geological mapping and earlier investigations. These zones also correspond with mineralisation geochemical fingerprints, resulting in multidisciplinary restrictions that reduce ambiguity in resistivity interpretation. This multievidence method guarantees that resistivity anomalies are not uncontrolled and are meaningfully related to subsurface geology, increasing confidence in finding mineralised structures within the anticlinorium. The topsoil curves illustrated in the figures demonstrate elevated resistivity values characteristic of the soil, implying the existence of lateritic horizons, frequently observed in tropical areas like the Benue Trough as a result of significant weathering processes. The Middle Layer Curves shown in figures 9 to 15 demonstrate low resistivity layers characteristic of clay-rich formations, including shales, commonly found in the Abakaliki Anticlinorium. Shales commonly act as host rocks for Pb-Zn mineralisation. The examination of the Deeper Layer Curves, as shown in figures 10 to 16, reveals that resistivity values in the study area rise fluctuates with depth (moderately high and low resistivity), a finding that is relevant to the Abakaliki Anticlinorium. This observation indicates that the Abakaliki Anticlinorium transitions from weathered shales to less weathered shales and more stable rocks capable of supporting mineral ores.

# Geological Importance of the study area

The resistivity patterns identified in the VES data are interpreted in light of known regional geological information of the Abakaliki Anticlinorium. Although direct drilling or 3D subsurface lithological data for the specific research area are sparse, published studies and borehole logs from surrounding areas in the Abakaliki region provide comparable lithological profiles that corroborate our view. These investigations document characteristic resistivity values for lithologies such as lateritic overburden, ferruginized clay, fissile and fractured shale, and limestone, which correlate to the resistivity strata reported in our work. Furthermore, seismic, magnetic, and geothermal examinations of the Abakaliki Anticlinorium region confirm the presence of structural features like as folds, faults, and intrusive bodies, which alter resistivity signatures [19-22]. As a result, the relationship between VES resistivity patterns and subsurface geology is supported by indirect but strong multidisciplinary evidence, giving considerable confidence in linking resistivity anomalies to recognised geological units and structures in the Abakaliki Anticlinorium. Future integration of precise drill data

J Earth Sci Bioin, 2025 Page 7 of 11

and 3D geological modelling is advised to improve and validate these conclusions. The presence of low- to moderate-resistivity zones at intermediate depths suggests the dominance of weathered and fractured shale units, characteristic of the Asu River Group in the Abakaliki Formation [1]. The uniform resistivity observed at greater depths supports the hypothesis of compact or minimally fragmented shale bedrock, typical of the deformed sedimentary phases in this region. The elevated resistivity zones observed near the surface, particularly at certain VES locations, suggest varied characteristics of the overburden, likely attributable to tectonic uplift, erosion, and differential weathering processes associated with the anticlinorium structure [13]. The findings highlight the impact of the region's tectonic history on current subsurface conditions. The findings suggest moderate groundwater potential, with aquifer zones likely located within the weathered and fractured shale formations. The clay-rich composition of these strata may limit aquifer productivity. The geoelectric signals support the established geological framework of the Abakaliki Anticlinorium, confirming the influence of Cretaceous deformation and sedimentation on the region's underlying characteristics [2].

# **Geochemical Analysis**

Pitting was conducted at the seven VES locations to the depth of 3m in the subsurface, and the collected samples underwent geochemical analysis. The X-ray fluorescence (XRF) analysis of the 7 PIT samples offers information about the fundamental components and mineral characteristics of the material. The analysis employed the Fundamental Parameters (FP) method, resulting in qualitative and quantitative information. The primary findings from the XRF analysis include the concentrations of major, minor, and trace oxides present in the samples [23].

#### PIT 1 Composition Analysis

This pit disclosed the following major, minor, and trace oxides in their respective proportions or concentrations. Three oxides were observed to be more prominent in the sample from pit 1. The sample comprises the following oxides: Silicon Dioxide (SiO<sub>2</sub>) at 60.79 wt.% (72.83 mole%), Ferric Oxide (Fe<sub>2</sub>O<sub>3</sub>) at 16.35 wt.% (7.37 mole%), and Aluminium Oxide (Al<sub>2</sub>O<sub>3</sub>) at 14.47 wt.% (10.21 mole%), representing the major oxides present. The minor oxides are present in the following concentrations: Magnesium Oxide (MgO) 1.07 wt.% (1.90 mole%), Calcium Oxide (CaO) 1.16 wt.% (1.49 mole%), Potassium Oxide (K2O) 1.35 wt.% (1.03 mole%), Titanium Dioxide (TiO<sub>2</sub>) 1.99 wt.% (1.79 mole%), Sulphur Trioxide (SO<sub>3</sub>) 0.80 wt.% (0.72 mole%), and Chlorine (Cl) 0.93 wt.% (1.88 mole%). Traces of the following oxides were identified – Vanadium (V) oxide (V<sub>2</sub>O<sub>5</sub>), Chromium (III) oxide (Cr<sub>2</sub>O<sub>3</sub>), Manganese (II) oxide (MnO), Copper (II) oxide (CuO), Lead (II) oxide (PbO), Cadmium (II) oxide (CdO), and Tantalum(V) oxide (Ta<sub>2</sub>O<sub>5</sub>), including Gold (Au). The results indicate the presence of a silica (SiO<sub>2</sub>) rich material, likely quartz. The analysis indicated a significant presence of iron ore and ironrich formations. The presence of Al<sub>2</sub>O<sub>3</sub> suggests the existence of clay minerals (alumino-silicates), whereas titanium and manganese indicate the potential for ilmenite and pyrolusite. Gold was present, albeit at a minimal concentration of 0.002 wt.%. The heavy metals Pb, Cd, and Cu have been identified and require assessment for their environmental impact.

#### **PIT 2 Composition Analysis**

The following are the principal oxides identified in PIT 2 (VES 2 site). - SiO<sub>2</sub> (55.527 wt.%) is the predominant oxide characteristic of sandstones or quartz-rich formations. Fe<sub>2</sub>O<sub>3</sub> (24.626 wt.%) indicates iron concentration, characteristic of ironstones or lateritic surfaces. TiO<sub>2</sub> (3.698 wt.%) signifies the presence of heavy minerals such as ilmenite, while Aluminum oxide (Al<sub>2</sub>O<sub>3</sub>) (10.477 wt.%) suggests clay-rich formations or

bauxitic alteration. The minor oxides included Calcium oxide (CaO) (1.680 wt%), indicating the presence of carbonates or small calc-silicates. Potassium oxide (K<sub>2</sub>O) (1.314 wt%) indicates the presence of feldspar or mica minerals, while Cl (0.999 wt%) suggests evaporite influence or fluid activity. CuO (0.089 wt%) contains trace oxides and elements, indicating the presence of mineralising fluids. Cobalt (II, III) oxide (Co<sub>3</sub>O<sub>4</sub>) (0.114 wt%) in geochemical samples serves as an indication or pathfinder for base metal mineralisation. Cobalt is typically found with economically important sulphide minerals such as copper and nickel, and its presence may indicate hydrothermal mineralising processes linked with base metal ore deposits. Thus, elevated levels of cobalt oxide in surface or subsurface samples can indicate the presence of underlying base metal mineralisation, leading mineral exploration operations [24-25]. Vanadium oxide (V2O5) at 0.173 wt% was found in organic-rich shale formations due to its ability to substitute into clay minerals and bind with organic materials inside shales. To show a strong relationship, V<sub>2</sub>O<sub>5</sub> concentrations must be closely correlated with shale content or proxies like clay mineral or total organic carbon content in samples. Zinc oxide (ZnO) at 0.028 wt% suggests the possibility of Pb-Zn mineralisation, whilst lead oxide (PbO) at 0.041% confirms the existence of lead, a key pathfinder element for mineralisation in this setting [26]. ZnO (0.028 wt%) suggests Pb-Zn mineralisation. PbO (0.041%) indicates the presence of lead, which is important in this context. Cadmium oxide (CdO) at 0.165% designates that cadmium frequently exist alongside zinc-lead ores, mostly substituting zinc in the mineral sphalerite, the main zinc ore mineral [27]. Nevertheless, this is an extensive geochemical connection, and showing mineralisation in surface rocks demands additional geological, mineralogical, and petrographic data. While high CdO concentrations infer geochemical attraction with Pb-Zn mineralisation, other surveys such as identification of ore minerals, structural controls, and mineralised textures are needed to reveal if the surface rocks are mineralised. A gold concentration of 0.011% is very low, approximating the detection limits of certain analytical processes. It is imperative to highlight that XRF's precision for gold at such low concentrations is inadequate, therefore results were taken with caution. Fire assays and ICP-MS are advised for more precise quantification of low-level gold. Elevated Fe2O3 levels signify areas of significant hydrothermal activity conducive to sulphide mineralisation. High levels of Potassium oxide (K<sub>2</sub>O) and Al<sub>2</sub>O<sub>3</sub> indicate the presence of clay-rich regions and hydrothermal alteration zones [28]. The existence of PbO, Cadmium oxide (CdO), and Zinc oxide (ZnO) indicates the potential for lead-zinc mineralisation. Evidence of copper (Cu) and gold (Au) suggests the presence of economically important minerals, though not in commercially viable quantities. The presence of chlorine in the samples indicates interaction with mineralising fluids; however, chlorine can also result from other processes such as diagenetic alteration or fluid-rock interaction that is unrelated to mineralisation. As a result, chlorine presence was interpreted cautiously and in conjunction with other geological and geochemical markers to indicate the existence of mineralising fluids [29-30].

#### PIT 3 Composition Analysis

The sample is primarily quartz, with 43.974% silicon dioxide (SiO<sub>2</sub>), typical of sandstones or quartz-rich deposits. Iron oxide (Fe<sub>2</sub>O<sub>3</sub>) concentration of 29.740% suggests hydrothermal alteration or iron enrichment. Aluminium oxide (Al<sub>2</sub>O<sub>3</sub>) concentration of 20.679% indicates clay-rich materials. 1.705% titanium dioxide (TiO<sub>2</sub>) content indicates the existence of titanium-bearing minerals like ilmenite. The presence of potassium oxide (K<sub>2</sub>O) at 1.623% suggests the presence of feldspar or mica, related to hydrothermal activities. Chlorine (Cl) at 0.887% suggests evaporation or chloride-rich fluid interactions. Copper oxide (CuO) at 0.048%

J Earth Sci Bioin, 2025 Page 8 of 11

suggests base metal mineralisation, Co<sub>3</sub>O<sub>4</sub> at 0.135% suggests base metal exploration, and V<sub>2</sub>O<sub>5</sub> at 0.110% implies organic-rich sediments. Lead oxide (PbO) at 0.028% is needed for Pb-Zn exploration, while cadmium oxide (CdO) at 0.048% belongs to zinc and lead deposits. Even if gold (Au) is trace at 0.021%, it is substantial. The presence of 0.009% zinc oxide (ZnO) suggests base metal mineralisation. The presence of high Fe<sub>2</sub>O<sub>3</sub> content indicates hydrothermal action, favouring sulphide mineralisation. High quantities of Al<sub>2</sub>O<sub>3</sub> and K<sub>2</sub>O suggest clay-rich lithologies and hydrothermal alteration zones. PbO, CdO, and ZnO suggest lead-zinc mineralisation in the region. Although small, trace amounts of Au and Cu suggest local enrichment in precious and base metals. The presence of chlorine suggests mineralising fluids during rock formation, indicating an oregenic geochemical environment.

# **PIT 4 Composition Analysis**

The sample's geochemical analysis indicates a siliceous sedimentary rock, likely quartz arenite or silicified shale, with a composition of 50.440 wt.% SiO<sub>2</sub>. Al<sub>2</sub>O<sub>3</sub> (17.671 wt.%) implies kaolinite or illite clay minerals. The Fe<sub>2</sub>O<sub>3</sub> composition of 22.377 wt.% supports ferruginization or iron-rich minerals like haematite. Calcium oxide (2.125 wt.%) suggests marl or limestone. The presence of K<sub>2</sub>O (2.816 wt.%) suggests potassium-rich minerals like feldspars or clays. In contrast, TiO<sub>2</sub> (2.235 wt.%) is linked to heavy minerals as rutile or ilmenite. Mineralisation potential in the basin is indicated by trace elements and minor oxides, including V<sub>2</sub>O<sub>3</sub>, Cr<sub>2</sub>O<sub>3</sub>, MnO, CuO, Nb<sub>2</sub>O<sub>3</sub>, ZnO, PbO, Arsenic trioxide (As<sub>2</sub>O<sub>3</sub>), and Au in the geochemical Hydrothermal changes are demonstrated by SO3 and P2O5, while higher chlorine levels may cause fluid inclusions or halite crystallisation. Lead, zinc, copper, and gold concentrations indicate polymetallic mineralisation zones similar to Pb-Zn-Au belts. Although elevated iron and manganese levels could indicate the presence of Fe-Mn nodules or ore bodies, no apparent Fe-Mn nodules were found in the analysed surface rocks. Iron and manganese are more likely to appear as finely scattered minerals or within the rock matrix than as distinct nodules. Trace levels of lead (Pb) and zinc (Zn) in the samples confirm a historical link to regional mineral belts characterised by Pb-Zn mineralisation, which is consistent with geological and geochemical characteristics observed in similar locations. Gold (Au) presence supports the possibility of hydrothermal gold mineralisation, as evidenced by related alteration minerals and geochemical evidence of hydrothermal activity throughout the basin. Titanite and pyrochlore may coexist due to their relationship with vanadium (V) and niobium (Nb). Titanite can incorporate Nb and V during hydrothermal alteration, whereas pyrochlore is a primary Nb-bearing mineral typically found in alkaline igneous rocks. The simultaneous increase in SiO<sub>2</sub>, Al<sub>2</sub>O<sub>3</sub>, and Fe<sub>2</sub>O<sub>3</sub> often reflects the impacts of diagenetic alteration and hydrothermal overprinting processes that affect the original rock chemistry. Zirconium and titanium indicate a stable heavy mineral matrix. The major element data suggests siliciclastic sedimentation with increased SiO2 and associated oxides, while trace elements and geochemical signals support hydrothermal mineralisation. Structural features found in the region suggest the occurrence of polymetallic vein systems controlled by local faults and fractures, which is consistent with regional geological models of the Abakaliki Anticlinorium [31-35].

# **PIT 5 Composition Analysis**

The geochemical analysis of PIT 5 reveals a siliceous composition, with 43.375 wt.% SiO<sub>2</sub> suggesting quartz-rich sedimentary rocks or silicification processes, and 16.154 wt.% Al<sub>2</sub>O<sub>3</sub> indicating the presence of clay minerals such as kaolinite and illite. The elevated Fe<sub>2</sub>O<sub>3</sub> content of 28.160 wt.% indicates substantial iron enrichment due to hydrothermal or ferruginization processes. Conversely, 7.052 wt.% MgO indicates the presence of dolomitic

or magnesium-rich clays. At 2.235 wt.% K<sub>2</sub>O, potassium feldspar or clay minerals such as illite are present, whereas 1.177 wt.% TiO<sub>2</sub> indicates the presence of heavy minerals like rutile and ilmenite. The existence of trace elements and minor oxides, including V<sub>2</sub>O<sub>5</sub>, Cr<sub>2</sub>O<sub>3</sub>, MnO, Co<sub>3</sub>O<sub>4</sub>, CuO, Niobium (III) oxide (Nb<sub>2</sub>O<sub>3</sub>), ZnO, PbO, and Au, suggests the possibility of mineralisation. The presence of SO<sub>3</sub> and P<sub>2</sub>O<sub>5</sub> indicates hydrothermal fluids, whereas the elevated Cl concentration implies saline- or brine-related fluids in mineralisation. Elevated amounts of iron, manganese, cobalt, copper, lead, and gold suggest hydrothermal mineralisation, which is characterised by mineral deposition from hot fluids, or supergene enrichment, which involves secondary metal concentration at the surface due to weathering and oxidation processes. These two processes are unique and require different types of evidence to be confirmed, such as alteration mineral assemblages for hydrothermal activity or weathering profiles and metal zoning patterns for supergene enrichment. The minor gold discovery indicates possibilities for geological exploration, whereas the PbO corresponds with the Pb-Zn mineral belts of the Abakaliki zone. The findings corroborate previous Pb-Zn mining and indicate Feoxide-associated and polymetallic sulphide mineralisation along fractures and fault zones. The amounts of iron and magnesium suggest hydrothermal alteration zones that may be linked to structural controls, while chlorine levels indicate mineralising fluids related to evaporites or brines. The geochemical composition indicates a hydrothermally altered siliciclastic sedimentary protolith that aligns with the tectono-sedimentary evolution and mineralisation patterns of the Abakaliki Anticlinorium.

#### PIT 6 Composition Analysis

The geochemical analysis of the rock sample from PIT 6 reveals a SiO2 content of 58.655 wt.%, suggesting the presence of siliceous rocks, including quartzites, cherts, or silicified shales. The detection of Al<sub>2</sub>O<sub>3</sub> at 16.964 wt.% indicates a clay mineral composition, specifically kaolinite and illite. The elevated Fe<sub>2</sub>O<sub>3</sub> concentration of 17.853 wt.% indicates iron enrichment derived from hydrothermal fluids. The presence of TiO2 at 1.488 wt.% indicates the existence of heavy minerals, such as rutile and ilmenite, within mature sedimentary rocks. K2O and CaO, at 1.574 wt.% and 0.531 wt.%, respectively, indicate minor contributions from potassium feldspar, illite, and potentially calcite. Trace elements such as V<sub>2</sub>O<sub>5</sub>, Cr<sub>2</sub>O<sub>3</sub>, Co<sub>3</sub>O<sub>4</sub>, NiO, CuO, ZnO, PbO, and Au suggest the potential for polymetallic mineralisation. The presence of SO<sub>3</sub> and P<sub>2</sub>O<sub>5</sub> indicates enrichment in sulphides and mild phosphates. Elevated Cl levels suggest the presence of saline fluids, whereas increased ZrO<sub>2</sub> enrichment reflects sedimentary maturity and a concentration of heavy minerals. The occurrence of Fe, V, Co, Cu, Pb, Zn, and Au indicates hydrothermal polymetallic sulphide veins with Pb-Zn mineralisation and secondary gold enrichment. Although BaO and sulphur-bearing elements may indicate barite mineralisation and a relationship between Fe-oxides and polymetallic deposits, no barite was visible in the samples. As a result, barite mineralisation inference is mostly reliant on geochemical markers and requires additional mineralogical confirmation. The geochemical profile indicates a siliciclastic sedimentary environment influenced by hydrothermal activity, akin to the lead-zinc-barite vein systems of the Abakaliki Anticlinorium.

# PIT & Composition Analysis

Geochemical analysis of PIT7's sample shows mineralisation potential in the study area. The XRS-FP XRF analysis reveals a siliceous to argillaceous lithology, with silica (SiO<sub>2</sub> at 58.12 wt.%) and alumina (15.86 wt.%), presumably from altered shale or tuffaceous Hydrothermal alteration, potentially driven by quartz veining or widespread silicification, is common in structurally deformed locations like the Abakaliki Anticlinorium. The high Fe<sub>2</sub>O<sub>3</sub> concentration (20.72 wt.%) suggests iron oxide

J Earth Sci Bioin, 2025 Page 9 of 11

mineralisation (e.g., haematite, goethite) or pyrite-rich layer alteration, exceeding typical shale levels. Due to trace levels of Cu (0.067 wt.%), Zn, Mn, Co, Ni, and Pb, hydrothermal iron migration may explain iron enrichment. These uncommon elements imply the occurrence of sulphide mineralisation systems, which could include volcanogenic massive sulphide (VMS) and sedimentary exhalative (SEDEX) types. While VMS and SEDEX deposits form in different ways-VMS deposits in volcanic undersea settings and SEDEX deposits in sedimentary basins—both involve submarine hydrothermal action during overlapping geological periods. The Benue Trough region has been shown to have coexisting VMS and SEDEX mineralisation, which is compatible with its complicated tectonic and sedimentary history. The occurrence of gold (Au) at 0.011 wt.% (110 ppm) and silver (Ag<sub>2</sub>O) at 0.051 wt.% (510 ppm) is economically significant. Although modest, these results are useful for geochemical reconnaissance. They may be associated with base metals in epithermal or mesothermal vein-type polymetallic systems in anticlinorial environments with structural complexity and fracture networks. Vein-hosted mineralisation is supported by hydrothermal fluid interaction with sedimentary host rocks, as seen in TiO<sub>2</sub> (1.53 wt.%) and trace elements, including V<sub>2</sub>O<sub>5</sub>, Cr<sub>2</sub>O<sub>3</sub>, and Nb<sub>2</sub>O<sub>3</sub>. Trace amounts of rare-metal pegmatitic veins or felsic intrusion enrichment, along with base and precious metals, may indicate a mineralised contact zone or alteration halo surrounding a deeper intrusive body [36-39]. High-tech businesses require tantalum and niobium, making small levels crucial for exploration. The overall geochemical profile matches Abakaliki Anticlinorium's Cretaceous marine shales, tectonic deformation, and intrusive formations. Hydrothermal alteration and mineral enrichment make the sampled area suitable for mineral exploration. Due to elemental connections, Gold - Silver (Au-Ag) veins, base metal sulphides, and rare metal pegmatites may be present.

#### Conclusion

This study confirms the effectiveness of integrating VES and XRF techniques for the identification of Pb-Zn mineralised zones in the Okokoma region. Future efforts must include drilling to validate geophysical interpretations and advanced mineralogical analyses to define ore textures. The integrated method provides a comprehensive, multidisciplinary framework to enhance mineral exploration in southeastern Nigeria. Geophysical investigations using Vertical Electrical Sounding (VES) and geochemical analyses through X-ray Fluorescence (XRF) in the study area have identified subsurface lithology, structural architecture, and mineralisation potential, aligning with the geological framework of the Abakaliki Anticlinorium. A geophysical investigation identified a four-layer geoelectric subsurface configuration. The elevated resistivity observed in the outermost layer (0-3 m) suggests the presence of dry, compacted lateritic topsoil or sandy/gravelly overburden. An intermediate zone, ranging from 3 to 8 meters in depth, exhibits moderate resistivity and is composed of sandy or silty clay along with partially weathered shale. A notable reduction in resistivity between 8 and 25 meters indicates the presence of worn, fractured, clay-rich shale, which serves as the main aquifer. Nonetheless, its composition may diminish groundwater yield. Layers ranging from 25 to 125+ meters exhibit consistently low resistivity, suggesting the presence of saturated compact shale or weakly fractured bedrock. Isolated high resistivity anomalies (VES 1, 2, 3, 5, 6, 7) are significant. The observed anomalies and curve forms indicate the presence of more competent rock, silicification, carbonate alteration, or structurally controlled features, such as faults and mineralised veins, that could contain ore deposits. The geochemical analysis of pit samples corroborated the geophysical results, revealing predominant oxides (SiO<sub>2</sub>, Fe<sub>2</sub>O<sub>3</sub>, Al<sub>2</sub>O<sub>3</sub>) in siliciclastic and clay-rich formations. The systematic identification of trace elements, such as Pb, Zn, Cu,

Au, Cd, Co, V, Nb, and Ta, at VES locations corroborates the geophysical detection of mineralisation. PbO, ZnO, and CdO indicate lead-zinc mineralisation, which corresponds with the Pb-Zn belts of the Abakaliki Anticlinorium. The presence of Au, Ag, and base metals indicates polymetallic sulphide veins and the enrichment of precious metals within epithermal or mesothermal systems. Elevated Fe<sub>2</sub>O<sub>3</sub> levels and chlorine concentrations suggest the presence of hydrothermal activity and the involvement of mineralising fluids. Integrated geophysical and geochemical data reveals lithologies, structural controls, hydrothermal alterations, and polymetallic mineralisation in the subsurface. This study enhances the geological understanding of the Abakaliki Anticlinorium and identifies areas with potential for mineral exploration, including lead, zinc, gold, silver, and possibly rare metals, thereby advocating for further research.

#### Acknowledgements

We want to acknowledge the Nigeria Geological Survey Agency for making available all the data used in this research available.

#### **Author contributions**

Chukwuebuka Nnamdi Onwubuariri and Istafanus Gwayeri Wasinda Conceptualized this research. The field Design was done by Istafanus Gwayeri Wasinda. The method for the research was initiated by Istafanus Gwayeri Wasinda and Chukwuebuka Nnamdi Onwubuariri. The original draft was carried out by Chukwuebuka Nnamdi Onwubuariri. The literature review was done by Paul Igienekpeme Aigba and Obinna Christian Dinneya. The final editing was done by Chukwuebuka Nnamdi Onwubuariri, alongside Istafanus Gwayeri Wasinda.

#### **Conflict of Interest Declaration**

There is none to declare

#### **Data Availability Declaration**

Data will be made available upon request

#### **Funding Statement**

No external funding received

#### References

abstract.

- Okoro A U, Ezeh H N (2024) Mineralogy and geochemical signatures for provenance and palaeoweathering conditions of the Upper Albian Abakaliki Shale, southeastern Nigeria. Geologos 30:169-186.
- 2. Okeke H C, Ehirim C N, Nwankwo L I (2023) Assessment of aquifer vulnerability in fractured rocks in the Abakaliki area, southeastern Nigeria, using geophysical and geological data. Environmental Earth Sciences 82: 10851.
- 3. Akiang F B, Amah E T, George A M, Agbasi O E (2024) Hydrogeological assessment and groundwater potential study in Calabar South Local Government Area: A vertical electrical sounding (VES) approach https://ui.adsabs.harvard.edu/abs/2025IJEWR...9..811A/
- 4. Osinowo O O, Ikhane P R (2023) Appraisal of geothermal potentials of some parts of the Abakaliki Anticlinorium and adjoining areas using magnetic data. Frontiers in Earth Science 11: 1216198.
- Onwubuariri C N, Ikeme C O, Ugochukwu J, Agoha C C, Ugwu J U et al. (2024a) Investigation and evaluation of aquiferous zones within Orlu and its environs, using a geo electrical and physiochemical approach. Archives of Advanced Engineering Science https://ojs.bonviewpress.com/index.php/AAES/article/view/2417.
- 6. Onwubuariri C N, Mgbeojedo T I (2018) Investigation of electrical properties of soil in relation to gully development

J Earth Sci Bioin, 2025 Page 10 of 11

- in Orlu, south eastern Nigeria. IOSR Journal of Applied Geology and Geophysics 6: 40-50.
- Ezekiel K, Garba M A, Hayatudeen M, Omang, B O (2023) Geophysical investigation of groundwater potentials using vertical electrical sounding: Case study of Boh Shongom Local Government Area, Gombe State, Nigeria. IRESPUB Journal of Natural & Applied Sciences 2: 1-15.
- 8. Ibrahim A, Omeneke A L, Aminu M B, Dung P D, Salisu S M et al. (2023) Application of vertical electrical sounding (VES) for the determination of water bearing zone in Karaworo, Lokoja, Kogi State, Nigeria. Journal of Geography, Environment and Earth Science International 27: 47-73.
- 9. Enciu A (2025) A novel 3D sampling method of geological rock core using X ray fluorescence http://arxiv.org/abs/2501.02366#:~:text=4%20Jan%20 2025%5D-,A%20novel%203D%20sampling%20 method%20of%20geological,core%20using%20X-ray%20 fluorescence&text=The%20current%20work%20 describes%20a,map%20of%20the%20scanned%20area.
- Lee S, Baur T, Clark J K, Emile Geay J (2024) MAX: Masked Autoencoder for X ray Fluorescence in geological investigation https://arxiv.org/html/2410.12330v1.
- 11. Abubakar A B, Anakwuba E K, Chukwuma O O (2024) Magnetic inversion modelling of subsurface geologic structures for mineral deposits mapping in southeastern Nigeria. Bulletin of the Mineral Research and Exploration 165-178.
- Onwubuariri C N, Agoha C C, Ikeme C O, Dinneya O, Emmanuel C e al. (2024b) Geophysical interpretation of Obudu area, Cross River State, southeastern Nigeria using aeromagnetic data. Acta Montanistica Slovaca 29: 787-803.
- 13. Afolabi O, Ogungbesan O A, Ajibade P A (2024) Mineralogy and geochemical signatures for provenance and palaeoweathering conditions of the upper Albian Abakaliki Shale in south eastern Nigeria. Geologos 30: 141-155.
- 14. Usman S O, Bawa Y, Adamu A, Eze A C (2024) Modelling the geothermal potentials energy of Abakaliki Lower Benue Trough Nigeria using Fourier transform of digital aeromagnetic data. International Journal of the Physical Sciences 19: 17-28.
- Onwubuariri C N, Agoha C C, Al Naimi L S, Mgbeojedo T I (2018b) Analyzing neo tectonic effects on gully development within Orlu and environs, south eastern Nigeria from Landsat imagery and azimuthal sounding data. International Journal of Development Research 8: 21038–21045.
- 16. Kabiri M, Ahmad M, Stott T (2024) X ray fluorescence core scanning for high resolution geochemical characterisation of soils. Soil Systems 8: 56.
- 17. Junussov Y, Mustapayeva M (2024) Preliminary XRF analysis of coal ash from Jurassic and Carboniferous coals at five Kazakh mines. Applied Sciences, 14(22), 10586.
- 18. Zhou, J., Tian, Y., Liu, Z., Zhang, B., Yu, W., & Song, B. (2023). The application of portable X ray fluorescence (pXRF) for elemental analysis of sediment samples in the laboratory and its influencing factors. Minerals 13: 989.
- 19. Ekwok P N, Ibe K M, Udo H E (2023) Geophysical characterization of subsurface structures in southeastern Nigeria. Journal of African Earth Sciences 190: 104632.
- 20. Ofoegbu C O (1991) Electrical and magnetic investigations for groundwater near the Obudu Plateau, southeastern Nigeria. Journal of African Earth Sciences 12: 231-240.

- 21. Egesi C N (2019) Hydrogeological study of fractured rock aquifers. Hydrogeology Journal 27: 1721-1734.
- 22. Ugodulunwa F N (2022) Structural framework and mineralization in Abakaliki area, Nigeria. Nigerian Journal of Geology 58: 45-56.
- 23. Murphy C, Pezic N (2023) Predictive geochemical exploration: Inferential generation of modern geochemical data and anomaly detection in legacy lake sediment surveys. Natural Resources Research 32: 4791-4816.
- 24. Wilburn K J (2013) Geophysical methods in mineral exploration. Exploration Geophysics 44: 123-131.
- 25. Konnunaho J P (2023) Advances in 3D geological modelling. Computers & Geosciences 170: 105026.
- Wu M, Zhang L, Li J (2021) Vanadium mineralisation in black shales. Ore Geology Reviews 134: 104064.
- 27. Schwartz T (2000) Trace element geochemistry of sphalerite in base metal deposits. Economic Geology 95: 953-967.
- 28. Onwubuariri C N, Ijeh B I, Anyadiegwu F C, Eze M O (2025)
  Assessment of geothermal energy potential of the Lower
  Benue Trough using integrated geophysical approach. Journal
  of the Indian Society of Remote Sensing
  https://link.springer.com/article/10.1007/s12524-024-02116-5
- Banks D A (2000) Hydrothermal alteration and geochemical signatures. Geochemistry, Geophysics, Geosystems 1: 102-115.
- 30. Tysdal R G (1997) Fluid histories and alteration in mineral deposits (U.S. Geological Survey Bulletin 2130-M). U.S. Geological Survey.
- 31. Leach D L (2001) Characteristics of sediment-hosted Pb-Zn deposits. Economic Geology, 96: 1127-1140.
- Zhang L (2008) Geochemistry and mineralisation of polymetallic deposits. Journal of Asian Earth Sciences 33: 480-491.
- 33. Salako OT, et al. (2024). Hydrothermal alteration in southwest Nigeria. Nigerian Journal of Mining and Geology 60: 180-191.
- Uzoegbu O C, Onwualu-John I J (2023) Structural control of mineral deposits in Abakaliki. Journal of Structural Geology 185: 104769.
- 35. Eges C N (2014) Mineralogical investigation of lead-zinc mineralisation. International Journal of Earth Sciences 103: 1713-1722.
- 36. Ekwueme B O (2017) Integrated geophysical and geochemical study of mineralisation zones. Journal of African Earth Sciences 131: 176-183.
- 37. Nnamani N, Onyia U (2020) Geochemical constraints on ore genesis in southeastern Nigeria. Ore Geology Reviews 118: 103374.
- 38. Coker K, Arne D C (2023) Stream sediment geochemistry in mineral exploration: A review of recent developments and applications. Geochemistry: Exploration, Environment, Analysis 23: 1-19.
- 39. Pan G, Huang L, Tang S, Yang J, Lu Y (2024) Mapping geochemical anomalies by accounting for the uncertainty of mineralization related elemental associations: A case study from the Sichuan Basin, China. Solid Earth 15: 731-748.
- 40. Drawell Analytical (2025) XRF analysis limitations in trace metal detection. Drawell Analytical Reports 12: 1-7.
- 41. Napcolab (2025) Limitations of XRF for gold assay. Napcolab Technical Bulletin 8.

Copyright: © 2025 Henghua Yan. This is an open-access article distributed under the terms of the Creative Commons Attribution License, which permits unrestricted use, distribution, and reproduction in any medium, provided the original author and source are credited.

J Earth Sci Bioin, 2025 Page 11 of 11